Magnetization reversal in epitaxial Fe nanowires on GaAs(110)

C. Hassel,* F. M. Römer, R. Meckenstock, G. Dumpich, and J. Lindner
Fachbereich Physik, Experimentalphysik, AG Farle, Universität Duisburg-Essen, Duisburg 47048, Germany
(Received 14 April 2008; revised manuscript received 15 May 2008; published 26 June 2008)

The anisotropy constants of epitaxial Fe films prepared on GaAs(110) are determined using ferromagnetic resonance. The films are structured into wires by employing electron-beam lithography with subsequent Argon-ion etching. Magnetoresistance measurements for wires with widths ranging from 250–2000 nm show the increasing influence of the shape anisotropy with decreasing wire widths. The magnetocrystalline anisotropy constants determined from these measurements agree well with the values obtained for the continuous films. These results are additionally confirmed by magnetic force microscopy measurements and micromagnetic simulations using the object oriented micromagnetic framework (OOMMF). We show that we are able to prepare wires with a remanent magnetization oriented perpendicular to their long axis due to the interplay of cubic and uniaxial in-plane magnetic anisotropies. Moreover, we can tune the effective easy axis by adjusting the width of the wires.

DOI: 10.1103/PhysRevB.77.224439 PACS number(s): 75.47.−m, 73.50.−h, 75.30.Gw, 75.60.Jk

I. INTRODUCTION

It has been shown that the magnetization reversal processes in single magnetic nanowires can be obtained by magnetoresistance measurements.[1] Since the electrical resistance depends on the angle between the magnetization and the current direction due to the anisotropic magnetoresistance,[2] various magnetization reversal processes can be distinguished.[3] Nanowires can be prepared using various methods, e.g., by lithography methods,[4] by electrodeposition via template assembly,[5] or by focused ion-beam technique.[6] Most of the magnetic nanowires, which have recently been investigated, are polycrystalline. In these wires the shape anisotropy dominates the magnetization reversal processes, since the magnetocrystalline anisotropy can be neglected due to randomly orientated grains. Thus, the easy axis of magnetization in polycrystalline nanowires is oriented along the wire axis, as has been shown by various authors for differently prepared nanowires.[7,8] On the other hand, it has been shown that magnetocrystalline anisotropy plays an important role in single crystalline nanowires, e.g., Co nanowires.[9,10] To obtain the magnetic properties of nanowires, nanowire gratings are often prepared, which allows the use of well-known techniques such as magneto-optical Kerr effect (MOKE), superconducting quantum interference device (SQUID), or ferromagnetic resonance (FMR). Single nanowires are more suitable to study their intrinsic magnetic properties. As has been shown previously, it is possible to determine magnetic anisotropies of single nanowires by magnetoresistance measurements.[11]

On the other hand, epitaxially prepared samples allow the determination of the magnetocrystalline anisotropy. However, epitaxial magnetic nanowires have to be prepared completely different as compared to polycrystalline samples, since one needs special condensation conditions, which are not compatible with various processes of structuring the samples.

Typically, arrays of patterned elements of epitaxially grown Fe on GaAs(100) have been investigated by MOKE (Ref. 12) and magnetoresistance.[3] The remanent states of patterned elements of Fe on GaAs(100), as well as on GaAs(110), were characterized by magnetic force microscopy (MFM).[13] Epitaxially grown Fe films in the (110) orientations exhibit magnetic anisotropy of uniaxial character within the film plane.[14]

In the present paper, we show results for epitaxial Fe films grown on (110) oriented GaAs substrates, which have been restructured into single nanowires using a specific electron-beam lithography (EBL) process. By varying the widths of the nanowires, we can tune the effective easy axis of magnetization, which leads for wide Fe wires to the extraordinary situation that the magnetization is oriented perpendicular to the wire axis even at remanence. The reason is that in this case the in-plane magnetocrystalline anisotropy is larger as compared to the shape anisotropy.

To determine the magnetization reversal processes, we performed magnetoresistance measurements in combination with FMR measurements on epitaxial Fe/GaAs(110) films. Furthermore, we performed micromagnetic calculations [object oriented micromagnetic framework (OOMMF) (Ref. 15)] and MFM measurements to confirm and support our experimental results.

II. EXPERIMENT DETAILS

The Fe films studied in this paper are prepared on commercial GaAs(110) wafers doped with Si. After an *ex situ* cleaning process in an ultrasonic bath, the substrates are transferred into an ultrahigh vacuum (UHV) chamber with a base pressure of 1×10^{-10} mbar. Subsequently, the substrates are cleaned by 1 h Ar sputtering with an energy of 0.5 keV. Afterwards, the substrates were annealed at 850 K for 30 min. After another short sputtering cycle (30 min), the samples were finally annealed for 45 min at 900 K. Auger electron spectra (AES) (not shown) clearly reveal that no carbon and oxygen contaminations are left on the substrate after the cleaning process. Figure 1(a) shows a typical low-energy electron diffraction (LEED) image, which was obtained from the GaAs(110) substrate after the cleaning process. The LEED pattern clearly reveals a well-ordered (110)

 ©2008 The American Physical Society

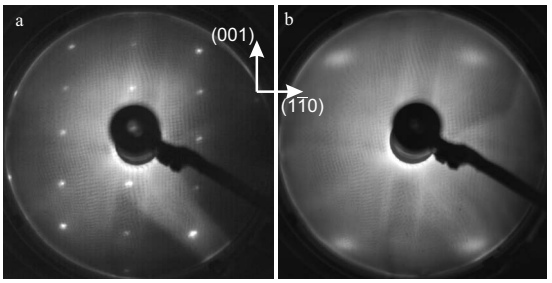

FIG. 1. LEED images at 195 eV of (a) the GaAs(110) substrate after the cleaning process. (b) 10 nm bcc-Fe film on the GaAs(110) substrate.

surface of the substrate with no surface reconstruction. Subsequently, Fe was evaporated from a four pocket *e*-beam evaporator with a deposition rate of approximately 0.1 nm/min. During growth, the substrates were held at room temperature. The thickness was monitored and determined using a quartz balance, which was calibrated using atomic force microscopy (AFM) and x-ray reflectometry measurements. The pressure during the evaporation was better than 8×10^{-10} mbar. The Fe films are free of contaminations, such as carbon and oxygen, as proven by AES.

Figure 1(b) shows a typical LEED pattern of an Fe film. The broad spots confirm the epitaxial growth of the Fe. The rectangular structure of the four spots with an aspect ratio of $\sqrt{2}$ reflects the elementary cell of a bcc (110) surface. Monitoring the intensity of the (0,0) spot as a function of the electron energy allows one to determine the vertical lattice parameter of the film. From this IV-LEED measurements, we determined the vertical lattice parameters for the GaAs(110) substrate, as well as for the Fe films. Whereas we observed a value for the substrate being very close to the literature value, we found that the Fe lattice parameter was systematically larger by 0.6% than the bulk value. This can be explained and is expected by the lateral lattice mismatch between the GaAs ($a_{\mathrm{GaAs}}=0.56537$ nm) and the Fe($2\cdot a_{\mathrm{Fe}}=0.57328$ nm). Since the Fe is compressed laterally, a vertical expansion occurs to minimize the elastic energy. From these measurements, we can deduce the epitaxial relation GaAs(110)[001]$\|$Fe(110)[001]. To protect the Fe films during the following process steps, the films were capped with 2 nm Ag, which is immiscible with Fe, and 3 nm Pt to prevent oxidation.

To characterize the magnetic properties of the films, FMR, as well as SQUID measurements, were carried out at room temperature.

After being magnetically characterized, the films were structured into wires with a length $l=60$ μm and widths varying from 250 nm to 2 μm using EBL. We spin coated a negative *e*-beam resist (Allresist AR-N 7520) onto the substrates. The resist was annealed for 2 min at 85 °C on a hot plate. After the exposure at a dose of 30 $\frac{\mu C}{cm^2}$ and subsequent development of the wire structures, the samples are inserted into another UHV chamber. There, 0.5 keV Ar ions are used for etching the nonprotected part of the Fe films. The remaining resist on the Fe structures is removed in an acetone bath. To perform magnetoresistance measurements in a four-point

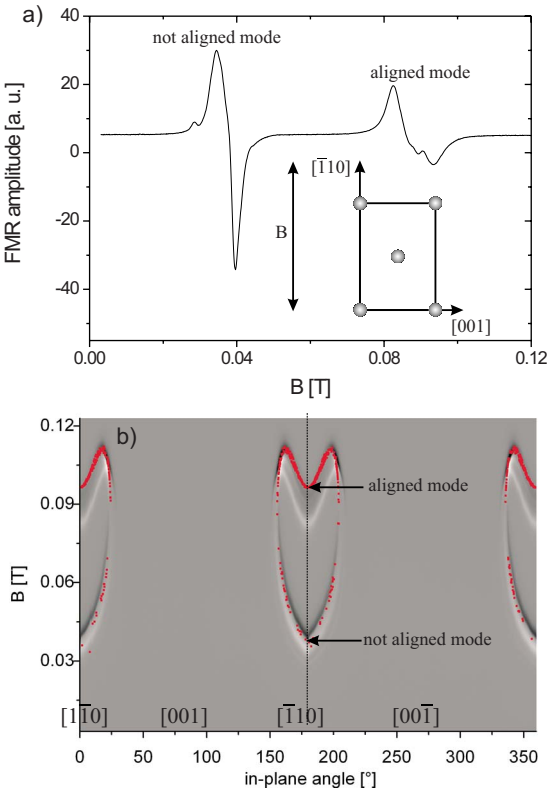

FIG. 2. (Color online) (a) Single FMR spectrum with the magnetic field applied along the $[\bar{1}10]$ direction. (b) Grayscale plot of the in-plane angular dependent FMR measurement of a 10-nm thick Fe film on GaAs(110). The square points are calculated using $k_1/M=21.3$ mT and $k_u/M=23.1$.

geometry, we contacted the Fe wires in a second EBL step with nonmagnetic gold wires of 100 nm thickness.[16] Here, we employed a conventional lift-off technique.

III. RESULTS AND DISCUSSION

From the SQUID data a saturation magnetization of $M_s=1640(80)$ kA/m was found, which is close to the bulk value of 1710 kA/m. The upper panel of Fig. 2 shows a FMR spectrum at a microwave frequency of 9.8 GHz, whereby the magnetic field is applied along the $[\bar{1}10]$ direction. The resonance at higher fields is the so-called aligned mode, where the magnetization precesses around the external magnetic-field direction, the resonance at low fields can be assigned to a so-called not-aligned mode (magnetization precession around internal anisotropy fields).[17] Within both modes, one can see small extra peaks. From spatially resolved FMR measurements performed in the center part of the film and at its rim, we can attribute these small extra resonances to excitations, which only occur at the rim of the film (for details on spatially resolved FMR, see Ref. 18). As only the center part was used for preparing the wires, we do not discuss the rim resonances in more detail.

To determine the anisotropy constants from FMR measurements, we obtained a full in-plane angular dependence of the FMR signal. This is plotted in Fig. 2(b) as a grayscale

plot. The dashed line indicates the position where the spectrum, shown in Fig. 2(a), was obtained. Bright gray contrast means positive FMR amplitude and dark gray contrast means negative FMR amplitude. Small dots are calculated points, as discussed below.

To calculate the expected resonance fields, we have to take into account the energy landscape of our sample. The free-energy density within a (110) plane is given by

$$F = -MB[\sin\theta\sin\theta_B\cos(\phi-\phi_B)+\cos\theta\cos\theta_B] - \left(\frac{1}{2}\mu_0 M_{\text{eff}}^2 - k_u\sin^2\phi\right)\sin^2\theta + \frac{k_1}{4}\left\{\cos^4\theta+\sin^4\theta[\sin^4\phi+\sin^2(2\phi)] + \sin^2(2\theta)\left(\cos^2\phi-\frac{\sin^2\phi}{2}\right)\right\} \quad (1)$$

Here ϕ (ϕ_B) denotes the in-plane angle between the magnetization (the external magnetic field) and the easy [001] direction, and θ (θ_B) is the polar angle of the magnetization (the external field) measured with respect to the film normal. The first term is the Zeeman contribution due to the external magnetic field, the second is the contribution due to shape anisotropy, the term including k_1 is the cubic anisotropy of the Fe, and the part including k_u is an additional uniaxial in-plane anisotropy with an easy axis parallel to the [001] direction. Note that such a contribution has also been reported by other groups.[14] Upon inserting the above free-energy density into the general expression for the FMR resonance condition (γ being the gyromagnetic ratio),[19]

$$\left(\frac{\omega}{\gamma}\right)^2 = \frac{1}{M^2\sin^2(\theta)}\left[\frac{\partial^2 F}{\partial\theta^2}\frac{\partial^2 F}{\partial\phi^2}-\left(\frac{\partial^2 F}{\partial\theta\,\partial\phi}\right)^2\right], \quad (2)$$

the whole in-plane angular dependence can be calculated, providing the aligned as well as the not-aligned mode. Note that the partial derivatives have to be evaluated at the equilibrium angles θ^{equ} and ϕ^{equ}, which minimize F. The fit to our data is shown as small dots within Fig. 2. We find a good agreement between measurements and calculation using the parameters $\frac{k_1}{M_S}=21.3(8)$ mT, $\frac{k_u}{M_S}=23.1(5)$ mT, and $M_{\text{eff}}=1530(30)$ kA/m. Using the saturation magnetization $M_S=1640$ kA/m, as determined by SQUID magnetometry, the anisotropy constants can be derived. We find a value of $k_1=3.5\times10^4\ \frac{J}{m^3}$, which is smaller compared to the Fe bulk value ($k_{1,\text{bulk}}=4.8\times10^4\ \frac{J}{m^3}$).

For the uniaxial anisotropy we find a value of $k_u=3.8\times10^4\ \frac{J}{m^3}$, which is a rather large value for a 10-nm thick film. Most likely, this high value arises from strain in the film rather than from pure interface effects. Note that since the easy axes of k_1 and k_u are parallel to the [001] direction, the total anisotropy is larger than for Fe bulk, which stabilizes the magnetization in that direction. The total anisotropy field of the film is thus $B_{a,\text{FMR}}=2(\frac{k_1}{M}+\frac{k_u}{M})=89$ mT. The results for the anisotropy constants are in good agreement with results from other groups for similar films.[13]

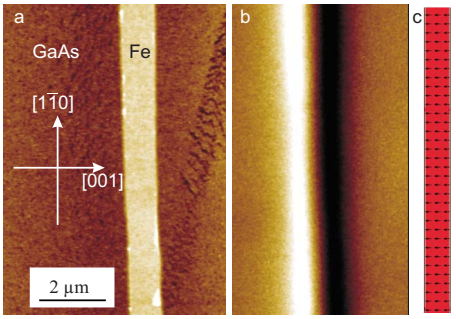

FIG. 3. (Color online) (a) AFM image of a typical wire. (b) MFM image after saturation of the wire in the [00$\bar{1}$] direction. (c) OOMMF simulation of the wire.

Note that the reduced value of M_{eff} compared to the saturation magnetization is due to a small contribution of a surface anisotropy which contributes to M_{eff}.

To examine the magnetic properties of single wires, we used MFM. Figure 3(a) shows an AFM image of a typical 1 μm-wide Fe wire prepared on GaAs. The long wire axis is orientated parallel to the intermediate [$\bar{1}$10] direction. Figure 3(b) shows an MFM image of the same wire after presaturation of the wire in a magnetic field applied parallel to the easy [00$\bar{1}$] direction. The image is then taken in remanence with an out-of-plane magnetized tip. One clearly observes a bright contrast on the left side of the wire indicating that stray field is leaving the sample plane and a dark contrast on the right side of the wire indicating that stray field is entering the sample plane. From this image, we can deduce that the magnetization in remanence is pointing along the [00$\bar{1}$] direction, i.e., transversal to the long wire axis. This experimental result is confirmed by micromagnetic simulations using the OOMMF program.[15] For the simulation we used the magnetic anisotropies, as determined by FMR. We used a cell size of 20×20 nm^2. The result of the OOMMF simulation is shown in Fig. 3(c), where arrows indicate the local magnetization direction. One can clearly see that the magnetization lies parallel to the magnetocrystalline easy direction, being oriented transversal to the long wire axis. This shows the dominating role of the intrinsic anisotropies as compared to the small shape anisotropy for broad wires.

Figure 4 shows the magnetoresistance at 4.2 K of a 2 μm-wide wire whose long wire axis is aligned parallel to the easy [001] direction and the magnetic field applied in plane and perpendicular to the wire axis. The arrows indicate the measurement sequence. Prior to the measurement, the wire was saturated along the [1$\bar{1}$0] direction. In remanence, the wire exhibits a high resistance. By applying a magnetic field along the [$\bar{1}$10] direction, the resistance decreases continuously at first until, at a field value of 77 mT, a strong decrease to the saturation value of the resistance is observed. Decreasing the field again, we find a hysteretic behavior for field values between 68 and 84 mT, while no hysteretic behavior is found in the other field regimes. This magnetoresistance behavior can be understood in terms of the anisotropic magnetoresistance (AMR).[2] Concerning the AMR, the resistance is high when the magnetization is oriented parallel

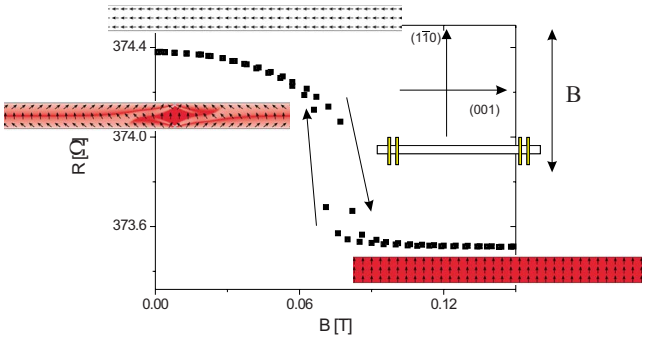

FIG. 4. (Color online) Magnetoresistance at 4.2 K of a 2 μm wide wire with the long wire axis parallel to the easy $[00\bar{1}]$ direction and the magnetic field applied parallel to the $[\bar{1}10]$ direction. The insets show OOMMF simulations at various magnetic fields. The sketch schematically shows the orientation of the wire and the magnetic field.

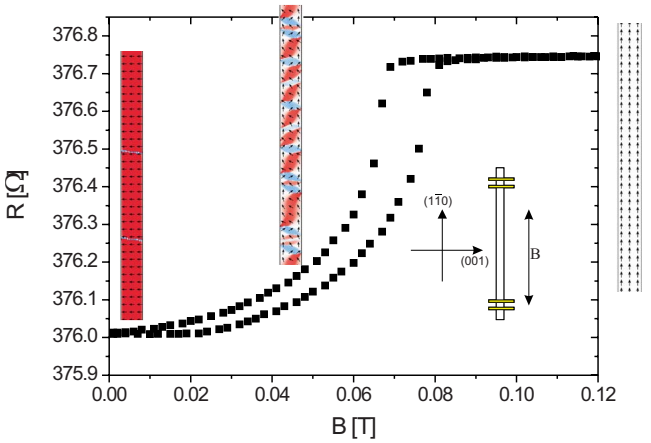

FIG. 5. (Color online) Magnetoresistance at 4.2 K of a 2 μm wide wire with the long wire axis parallel to the $[\bar{1}10]$ direction and the magnetic field applied parallel to the $[\bar{1}10]$ direction. The insets show OOMMF simulations at various magnetic fields.

to the current direction, i.e., the long wire direction. From this one can conclude that a remanent state pointing along the long wire axis exists. The behavior is expected due to the fact that the long wire axis is the easy direction for the shape, as well as the magnetocrystalline anisotropy. By applying small magnetic fields, we find a reversible behavior of the magnetoresistance, implying a coherent rotation of the magnetization without domain formation toward the magnetic-field direction. The sharp decrease in the resistance can be explained by considering that the hard $[\bar{1}11]$ direction lies between the [001] and the $[\bar{1}10]$ direction. When the magnetic field is sufficient to overcome the energy barrier, the magnetization switches into the magnetic-field direction. From the resistance value at the point where the sharp decrease starts, one can deduce an angle of 38(5)° between the magnetization and the current direction, since the resistance is given by the well-known $\cos^2$ behavior of the AMR.[2] This value can be confirmed by taking into account the free-energy density F given by Eq. (1), from which we can derive an angle of 38° as equilibrium angle for the magnetization direction, when the energy barrier from the $[\bar{1}11]$ direction vanishes. The magnetization reversal behavior is thus in good agreement with the expectation resulting from the analysis of the free-energy density of the system.

The saturation is achieved at a field of $B=B_a+B_S=84$ mT, which is the anisotropy field of the film B_a plus the shape anisotropy of the wire B_S.

We also note that the total relative resistance change of 0.23% agrees very well with findings from other groups for thin Fe films.[20]

The described magnetization reversal behavior can also be confirmed by OOMMF simulations (see insets). Calculating the remanent state of the wire using the anisotropy constants determined with FMR, we find a remanent state that points along the long wire axis (upper inset). The arrows indicate the local magnetization direction. For more clarity, the magnetization components pointing in the two in-plane transversal directions are indicated by the red and blue background color, respectively. White background means that the magnetization is pointing in the longitudinal direction. As one can see from the upper inset in Fig. 4, we find no transversal component of the magnetization in remanence. For small applied magnetic fields (middle inset), we find a state where the magnetization is rotated toward the magnetic-field direction, which can be seen by the red background. However, the rotation of the magnetization is not homogeneous inside the wire. Although we have large parts of the wire, where the magnetization rotates coherently, the rotation of the magnetization is in the middle part (not homogeneous). The lower inset shows the wire in the fully saturated state.

Figure 5 shows the magnetoresistance of a 2 μm-wide wire with the long wire axis being parallel to the $[\bar{1}10]$ direction and the magnetic field applied in the same direction. In remanence, we observed a low resistance. By increasing the magnitude of the magnetic field, the resistance increases continuously until it saturates. By decreasing the field, we find a hysteretic behavior of the resistance. This implies that we have (in remanence) a magnetization that lies transversal to the long wire axis even when the wire was presaturated longitudinal to the wire. The hysteretic resistance increase can be explained by domain formation during the magnetization reversal process. The saturation field in this case is $B=B_a-B_S=78$ mT, which is the anisotropy field of the film minus the shape anisotropy. Thus, comparing our magnetoresistance measurements shown in Figs. 4 and 5, we can derive an anisotropy field for the crystalline anisotropies of $B_{a,\mathrm{MR}}=81$ mT, which is in reasonable agreement with the FMR data $B_{a,\mathrm{FMR}}=89$ mT.

Also for this orientation of the wire, we conducted OOMMF calculations shown as insets in Fig. 5. The left inset shows the remanent state of the wire after saturation in the longitudinal direction. Here, we can see that the major part of the magnetization points transversal. By applying magnetic fields along the wire axis, the calculations yield strong domain formation in the wire (middle inset), which can be seen by the alternating red and blue contrast in the wire. Thus, this confirms that we have here no coherent rotation of magnetization. The right inset shows the wire in the saturated state.

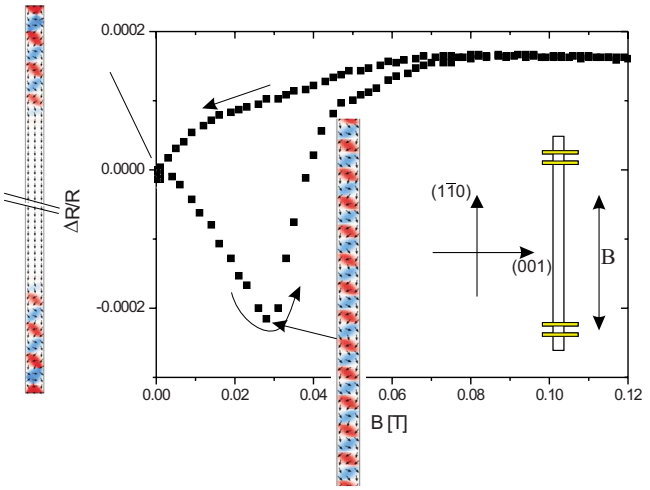

FIG. 6. (Color online) Magnetoresistance at 4.2 K of a 250 nm wide wire with the long wire axis parallel to the [$\bar{1}$10] direction and the magnetic field applied parallel to the [$\bar{1}$10] direction. The insets show OOMMF simulations at various magnetic fields.

Figure 6 shows the magnetoresistance of a wire in the same orientation as the wire in Fig. 5. However, this wire has a width of only 250 nm. One clearly observes a different behavior of the magnetoresistance. Starting from remanence, the resistance decreases and after a minimum, increases to a value that is higher than the remanent value. By decreasing the magnetic field, the resistance continuously decreases until remanence. This magnetoresistance behavior resembles that of broad polycrystalline Co wires[7] and this means that the effective easy axis of magnetization is here—in contrast to the 2 μm-wide wire shown in Fig. 5—oriented along the long wire axis. Thus, the shape anisotropy has overcome the magnetocrystalline anisotropy. This shows that varying the widths of the wires allows tuning of the effective magnetic anisotropies.

By applying a magnetic field, additional domains and thus transverse magnetization components are nucleated within the wire, which decreases the resistance due to the AMR. After the minimum, the magnetization slowly orientates longitudinal to the wire axis until it saturates. Obviously, the resistance at saturation is larger than the resistance in remanence. Thus, in remanence transversal components, different to the wires with a width of 2 μm, exist. This implies that the effective anisotropy is small and shows that for smaller Fe wires the shape anisotropy plays an important role.

The upper inset in Fig. 6 shows the OOMMF calculation for the remanent state of the wire. Here, we find some domain formation at the ends of the wire, but no domain formation in the central part of the wire. Due to our contacting process, we do not measure the resistance of the very end of the wire, but only 5 μm apart from the end. By increasing the field, the domain formation increases through the whole wire, which increases the transversal oriented part of the magnetization in the central part of the wire (lower inset).

In conclusion, we have prepared epitaxial wires of Fe on GaAs(110) in different orientations of the wires with respect to the crystallographic directions. For different orientations, we observe a different magnetoresistance behavior, which can be explained by different magnetization reversal processes that are in good agreement with OOMMF simulations. Reducing the wire width, we can change the effective easy axis of magnetization, when the shape anisotropy overcomes the crystalline anisotropy. The deduced anisotropy constants agree well with the anisotropy constants determined by ferromagnetic resonance.

ACKNOWLEDGMENTS

We thank the Deutsche Forschungsgemeinschaft for financial support through Grant No. SFB 491.

*christoph.hassel@uni-due.de

[1] K. Hong and N. Giordano, J. Magn. Magn. Mater. **151**, 396 (1995).
[2] T. R. McGuire and R. I. Potter, IEEE Trans. Magn. **11**, 1018 (1975).
[3] S. J. Blundell, C. Shearwood, M. Gester, M. J. Baird, J. A. C. Bland, and H. Ahmed, J. Magn. Magn. Mater. **135**, L17 (1994).
[4] M. Brands, C. Hassel, A. Carl, and G. Dumpich, Phys. Rev. B **74**, 033406 (2006).
[5] K. Nielsch, F. Müller, A.-P. Li, and U. Gösele, Adv. Mater. (Weinheim, Ger.) **12**, 582 (2000).
[6] J. Ferré, R. Hyndman, V. Repain, A. Mougin, J. P. Jamet, J. Gierak, D. Mailly, C. Chappert, V. Mathet, P. Warin, and J. Chapman, Trans. Magn. Soc. Jpn. **2**, 175 (2002).
[7] M. Brands, R. Wieser, C. Hassel, D. Hinzke, and G. Dumpich, Phys. Rev. B **74**, 174411 (2006).
[8] A. O. Adeyeye, J. A. C. Bland, C. Daboo, and D. G. Hasko, Phys. Rev. B **56**, 3265 (1997).
[9] U. Ebels, A. Radulescu, Y. Henry, L. Piraux, and K. Ounadjela, Phys. Rev. Lett. **84**, 983 (2000).
[10] L. Piraux, A. Encinas, L. Vila, S. Mátéfi-Tempfli, M. Mátéfi-Tempfli, M. Darques, F. Elhoussine, and S. Michotte, J. Nanosci. Nanotechnol. **5**, 372 (2005).
[11] M. Brands and G. Dumpich, J. Appl. Phys. **98**, 014309 (2005).
[12] U. Ebels, A. O. Adeyeye, M. Gester, R. P. Cowburn, C. Daboo, and J. A. C. Bland, Phys. Rev. B **56**, 5443 (1997).
[13] R. Pulwey, M. Zölfl, G. Bayreuther, and D. Weiss, J. Appl. Phys. **91**, 7995 (2002).
[14] J. J. Krebs, F. J. Rachford, P. Lubitz, and G. A. Prinz, J. Appl. Phys. **53**, 8058 (1982).
[15] http://math.nist.gov/oommf/
[16] M. Brands and G. Dumpich, J. Phys. D **38**, 822 (2005).
[17] R. Meckenstock, I. Barsukov, O. Posth, J. Lindner, A. Butko, and D. Spoddig, Appl. Phys. Lett. **91**, 142507 (2007).
[18] R. Meckenstock, Rev. Sci. Instrum. **79**, 041101 (2008).
[19] *Ultrathin Magnetic Structures II: Measurement Techniques and Novel Magnetic Properties*, 2nd ed., edited by B. Heinrich and J. A. C. Bland (Springer, Berlin, 2005).
[20] K. T. Riggs, E. D. Dahlberg, and G. A. Prinz, Phys. Rev. B **41**, 7088 (1990).